

Presentation of the Berry-Tabor conjecture in Lévy plates

Chao Li(李超) and Guo-Lin Hou(侯国林)

Citation: Chin. Phys. B, 2024, 33 (**10**): 104204. DOI: 10.1088/1674-1056/ad21f2
Journal homepage: http://cpb.iphy.ac.cn; http://iopscience.iop.org/cpb

What follows is a list of articles you may be interested in

Tunable phonon-atom interaction in a hybrid optomechanical system

Yao Li(李耀), Chuang Li(李闯), Jiandong Zhang(张建东), Ying Dong(董莹), and Huizhu Hu(胡慧珠)
Chin. Phys. B, 2023, 32 (**4**): 044213. DOI: 10.1088/1674-1056/acb9ea

Generation of atomic spin squeezing via quantum coherence: Heisenberg-Langevin approach

Xuping Shao(邵旭萍)
Chin. Phys. B, 2020, 29 (**12**): 124206. DOI: 10.1088/1674-1056/abab7c

A two-mode squeezed light based on a double-pump phase-matching geometry

Xuan-Jian He(何烜坚), Jun Jia(贾俊), Gao-Feng Jiao(焦高锋), Li-Qing Chen(陈丽清), Chun-Hua Yuan(袁春华), Wei-Ping Zhang(张卫平)
Chin. Phys. B, 2020, 29 (**7**): 074207. DOI: 10.1088/1674-1056/ab8abd

Stable continuous-wave single-frequency intracavity frequency-doubled laser with intensity noise suppressed in audio frequency region

Ying-Hao Gao(高英豪), Yuan-Ji Li(李渊骥), Jin-Xia Feng(冯晋霞), Kuan-Shou Zhang(张宽收)
Chin. Phys. B, 2019, 28 (**9**): 094204. DOI: 10.1088/1674-1056/ab327b

Tripartite continuous-variable entanglement of NOPA system

Chao-Ying Zhao(赵超樱), Cheng-Mei Zhang(张成梅)
Chin. Phys. B, 2018, 27 (**8**): 084204. DOI: 10.1088/1674-1056/27/8/084204

Presentation of the Berry–Tabor conjecture in Lévy plates

Chao Li(李超) and Guo-Lin Hou(侯国林)[†]

School of Mathematical Sciences, Inner Mongolia University, Hohhot 010021, *China*

(Received 10 October 2023; revised manuscript received 14 December 2023; accepted manuscript online 24 January 2024)

The Berry–Tabor (BT) conjecture is a famous statistical inference in quantum chaos, which not only establishes the spectral fluctuations of quantum systems whose classical counterparts are integrable but can also be used to describe other wave phenomena. In this paper, the BT conjecture has been extended to Lévy plates. As predicted by the BT conjecture, level clustering is present in the spectra of Lévy plates. The consequence of level clustering is studied by introducing the distribution of nearest neighbor frequency level spacing ratios $P(\tilde{r})$, which is calculated through the analytical solution obtained by the Hamiltonian approach. Our work investigates the impact of varying foundation parameters, rotary inertia, and boundary conditions on the frequency spectra, and we find that $P(\tilde{r})$ conforms to a Poisson distribution in all cases. The reason for the occurrence of the Poisson distribution in the Lévy plates is the independence between modal frequencies, which can be understood through mode functions.

Keywords: Berry–Tabor conjecture, frequency spectra, Hamiltonian approach, Lévy plates

PACS: 42.50.Lc, 47.10.Df, 33.20.Tp **DOI:** 10.1088/1674-1056/ad21f2

1. Introduction

Theories such as random-matrix theory,[1] periodic orbits,[2] and spectral statistics[3] have been developed to understand quantum systems whose classical counterparts are integrable or chaotic for decades. The research findings revealed that avoided crossings are present in chaotic wave systems and absent in integrable wave systems. The BT conjecture[4,5] and the Bohigas–Giannoni–Schmit (BGS) conjecture[6] explained that the reason for avoided crossings was level repulsion, which depends on the interaction between different energy levels. According to the BT conjecture, in quantum systems whose classical counterparts were integrable, the levels are uncorrelated, which leads to the absence of level repulsion, so the spectral fluctuations follow a Poisson distribution. The BGS conjecture pointed out that, due to level repulsion, the spectral fluctuations of quantum systems whose classical counterparts were chaotic could be predicted by the Gaussian orthogonal ensemble (GOE) of random-matrix theory. The Wigner surmise[7] $P_{\mathrm{W}}(s) = As^{\beta}\exp(-Bs^2 - Cs)$, where s represents the distance between two consecutive levels, and A, B, C are normalization constants, provided an appropriate expression for the two conjectures. When $\beta = 0$, $P_{\mathrm{W}}(s)$ follows a Poisson distribution, which means there is no level repulsion and is consistent with the BT conjecture. The other values of β (1, 2, and 4) in chaotic systems represented varying degrees of level repulsion according to the BGS conjecture.

The BT conjecture and the BGS conjecture not only successfully described the spectral fluctuations for quantum systems such as the Sinai billiard and Bunimovich stadium but they can also be applied to other wave systems, for instance, high-frequency resonance in microwave cavities.[8,9] Although research on vibrating plates has a long tradition[10–14] and some researchers have tried to do research in the wave chaos context,[15–19] the precise nature of wave chaos is still a highly open question in rectangular plates. Recently, Ref. [20] used finite element simulation software to obtain the frequency spectra and the distribution of nearest neighbor frequency level spacing $P(s)$ for rectangular plates with four free edges (FFFF) and four simply supported edges (SSSS). For the FFFF plate, avoided crossings are present in the frequency spectra, and the fluctuation of $P(s)$ is similar to certain transition distributions between GOE and Poisson distribution. For the SSSS plate, the avoided crossings are absent in the frequency spectra, and $P(s)$ follows a Poisson distribution. This was a significant attempt to discuss the plate vibration problem from the perspective of the BT conjecture and the BGS conjecture, opening new doors for our understanding of the free vibration of the plate.

Lévy plates are a particular class of rectangular thin plates with two opposite edges simply supported, while the other edges are a combination of clamped supported, simply supported, and free supported.[21] Up to this point, due to the complexity of the vibration problem for Lévy plates, the spectra of plates under combined boundary conditions have not been obtained entirely, and the influence of rotary inertia and foundation parameters on the spectra has yet to be studied. In this paper, using the Hamiltonian approach, we have obtained the analytical solution for the free vibration of Lévy plates on a two-parameter elastic foundation. Using the solutions we obtained, we plot the spectra for the 108 combinations of rotation inertia, foundation parameters, and boundary conditions and explore the effects of rotary inertia, foundation parameters, and boundary conditions on the shape of the frequency spectra. It should be noted that we improve the spectra by

[†]Corresponding author. E-mail: smshgl@imu.edu.cn

© 2024 Chinese Physical Society and IOP Publishing Ltd

introducing the aspect ratio and non-dimensional frequency parameter to make it more general. As predicted by the BT conjecture, level clustering appears in the frequency spectra. In order to identify the cause of level clustering, we have calculated $P(\tilde{r})$ for each of these cases and have found that $P(\tilde{r})$ is the same as a Poisson distribution. Additionally, we determine the minimum sample size required to display the shape of a Poisson distribution. In the end, we explain that the reason for $P(\tilde{r})$ following a Poisson distribution in Lévy plates is the independence of modal frequencies which can be understood through mode functions.

2. Analytic free vibration solution for Lévy plates

Figure 1 shows that the Lévy plates on a two-parameter elastic foundation are placed in a three-dimensional Cartesian coordinate system. According to the Kirchhoff–Love theory, the free vibration equation of thin plates on a two-parameter foundation derived by Hetényi's suggestion can be set as[22,23]

$$D\nabla^4 w + k_1 w - k_2\nabla^2 w - I\frac{\partial^2}{\partial t^2}\nabla^2 w + \rho h\frac{\partial^2 w}{\partial t^2} = 0, \tag{1}$$

where $D = Eh^3/[12(1-\nu^2)]$ is the flexural rigidity of the plate, $\nabla^4 = \nabla^2\nabla^2$ and $\nabla^2 = \partial^2/\partial^2 x + \partial^2/\partial^2 y$ is the Laplace operator, $I = \rho h^3/12$ is the rotary inertia, and k_1 and k_2 are the Winkler parameter and shear parameter of the foundation, respectively.

The transverse deflection in harmonic vibration can be set as

$$w(x,y,t) = W(x,y)\,\mathrm{e}^{\mathrm{i}\omega t}, \tag{2}$$

where ω is the natural angular frequency of the vibration and $W(x,y)$ is the mode function of the vibration. Substituting Eq. (2) into Eq. (1) we can get

$$D\nabla^4 W + k_1 W - k_2\nabla^2 W + I\omega^2\nabla^2 W - \rho h\omega^2 W = 0. \tag{3}$$

Importing Eq. (3) into the Hamiltonian system we can get[24–26]

$$\frac{\partial \boldsymbol{U}}{\partial y} = \boldsymbol{H}\boldsymbol{U}, \tag{4}$$

where

$$\boldsymbol{H} = \begin{pmatrix} \boldsymbol{0} & \mathcal{A} \\ \mathcal{B} & \boldsymbol{0} \end{pmatrix},$$

$$\mathcal{A} = \begin{pmatrix} 0 & 1 \\ 1 & -k_2 + I\omega^2 + \dfrac{2D(-1+\nu)}{\nu}\dfrac{\partial^2}{\partial x^2} \end{pmatrix},$$

$$\mathcal{B} = \begin{pmatrix} k_1 - k_2\dfrac{\partial^2}{\partial x^2} + \left(I\dfrac{\partial^2}{\partial x^2} - h\rho\right)\omega^2 + \dfrac{D(-1+\nu^2)}{\nu^2}\dfrac{\partial^4}{\partial x^4} & -\dfrac{1}{\nu}\dfrac{\partial^2}{\partial x^2} \\ -\dfrac{1}{\nu}\dfrac{\partial^2}{\partial x^2} & -\dfrac{1}{D} \end{pmatrix}$$

and

$$\boldsymbol{U} = \left(W \;\; M \;\; V \;\; \theta\right)^{\mathrm{T}},$$

$$M = -\frac{D}{\nu}\left(\frac{\partial^2 W}{\partial x^2} + \nu\frac{\partial^2 W}{\partial y^2}\right),$$

$$V = k_2\frac{\partial W}{\partial y} + D\left(\frac{1-2\nu}{\nu}\right)\frac{\partial^3 W}{\partial x^2\partial y} - D\frac{\partial^3 W}{\partial y^3}, \quad \theta = \frac{\partial W}{\partial y}.$$

The method of separating variables is valid for Eq. (4) in the symplectic geometry,[27] so that

$$\boldsymbol{U} = \boldsymbol{Z}(x)\boldsymbol{T}(y). \tag{5}$$

Substituting Eq. (5) into Eq. (4), we can obtain

$$\frac{\mathrm{d}Y(y)}{\mathrm{d}y} = \mu Y(y), \tag{6}$$

$$(\boldsymbol{H} - \mu\boldsymbol{I})\boldsymbol{Z}(x) = 0, \tag{7}$$

where $\boldsymbol{I}$ is the fourth order identity matrix, μ and $\boldsymbol{Z}(x)$ are the eigenvalue and eigenvector, respectively, and in the meantime $\boldsymbol{Z}(x)$ can be set as $\boldsymbol{Z}(x) = (Z_1(x), Z_2(x), Z_3(x), Z_4(x))^{\mathrm{T}}$.

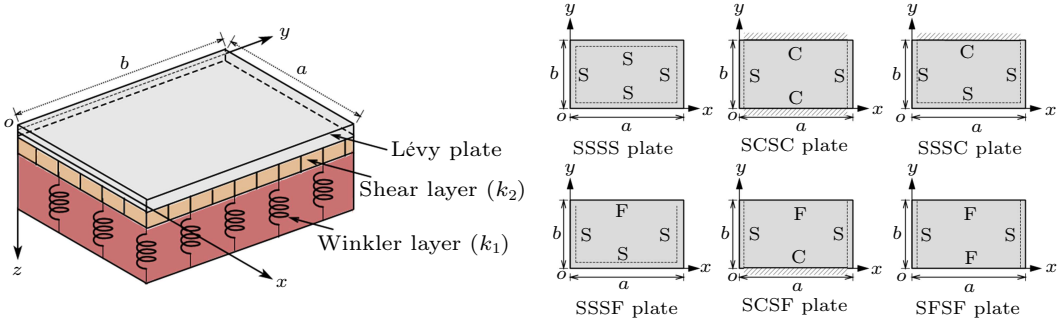


Fig. 1. Lévy plates on a two-parameter elastic foundation with six combinations of boundary conditions.

Substituting matrix $\boldsymbol{H}$ and vector $\boldsymbol{Z}(x)$ into Eq. (7) by simplification, we can get

$$D\frac{\mathrm{d}^4 Z_1(x)}{\mathrm{d}x^4}+\left(-k_2+I\omega^2+2D\mu^2\right)\frac{\mathrm{d}^2 Z_1(x)}{\mathrm{d}x^2}+\left(k_1-k_2\mu^2-\rho h\omega^2+I\omega^2\mu^2+D\mu^4\right)Z_1(x)=0. \quad (8)$$

The general solution of the differential Eq. (8) can be set as

$$Z_1(x)=C_1\mathrm{e}^{\lambda_1 x}+C_2\mathrm{e}^{\lambda_2 x}+C_3\mathrm{e}^{\lambda_3 x}+C_4\mathrm{e}^{\lambda_4 x}. \quad (9)$$

The boundary conditions of two opposite edges simply supported at $x=0$ and $x=a$ are

$$W|_{x=0,a}=0,\quad \left(\frac{\partial^2 W}{\partial x^2}+v\frac{\partial^2 W}{\partial y^2}\right)\Big|_{x=0,a}=0. \quad (10)$$

Substituting Eq. (9) into Eq. (10) we can get the eigenvalues

$$\mu_{n1}=\sqrt{\frac{2s+2D\alpha_n^2-I\omega^2-Q}{2D}},\quad \mu_{n2}=-\mu_{n1},$$
$$\mu_{n3}=\sqrt{\frac{2s+2D\alpha_n^2-I\omega^2+Q}{2D}},\quad \mu_{n4}=-\mu_{n3}, \quad (11)$$

where $Q=\sqrt{(-2s+I\omega^2)^2-4D(k-h\rho\omega^2)}$ and $\alpha_n=n\pi/a, n=1,2,3\ldots$ And the eigenvector we can get as

$$\boldsymbol{Z}_{ni}(x)=\begin{pmatrix}1\\ \dfrac{D\left(\alpha_n^2-v\mu_{ni}^2\right)}{v}\\ -\dfrac{\mu_{ni}\left(-2sv+Iv\omega^2+D\left((1-2v)\alpha_n^2+v\mu_{ni}^2\right)\right)}{v}\\ \mu_{ni}\end{pmatrix}\times\sin(\alpha_n x), \quad (12)$$

where $i=1,2,3,4$ and $n=1,2,3,\ldots$

Due to the simply supported boundary condition, the eigenvectors satisfy the symplectic orthogonality and completeness, so the state vector $\boldsymbol{U}$ can be expanded through symplectic eigenfunctions as[28]

$$\boldsymbol{U}(x,y)=\sum_{n=1}^{\infty}\left(\sum_{i=1}^{4}\boldsymbol{Z}_{ni}(x)\boldsymbol{Y}_{ni}(y)\right). \quad (13)$$

The first component of vector $\boldsymbol{U}(x,y)$ is $W(x,y)$ so the general solution we obtained is[29,30]

$$W(x,y)=\sum_{n=1}^{\infty}\left(C_{n1}\mathrm{e}^{u_{n1}}+C_{n2}\mathrm{e}^{u_{n2}}+C_{n3}\mathrm{e}^{u_{n3}}+C_{n4}\mathrm{e}^{u_{n4}}\right)\sin(\alpha_n x), \quad (14)$$

where C_{ni} $(i=1,2,3,4)$ are constants which can be obtained by the boundary conditions at sides $y=0$ and $y=b$. Substituting Eq. (14) into the boundary conditions in Table 1 leads to the desired frequency equations.

Case of the SSSS plate:

$$\sinh(b\mu_{n1})\sinh(b\mu_{n3})=0. \quad (15)$$

Case of the SCSC plate:

$$2\mu_{n1}\mu_{n3}-2\cosh(b\mu_{n1})\cosh(b\mu_{n3})\mu_{n1}\mu_{n3}+\sinh(b\mu_{n1})\sinh h(b\mu_{n3})\left(\mu_{n1}^2+\mu_{n3}^2\right)=0. \quad (16)$$

Case of the SSSC plate:

$$\mu_{n1}\cosh(b\mu_{n1})\sinh(b\mu_{n3})-\mu_{n3}\sinh(b\mu_{n1})\cosh(b\mu_{n3})=0. \quad (17)$$

Case of the SSSF plate:

$$\begin{aligned}&(v-2)v\alpha_n^4(\mu_{n1}\cosh(b\mu_{n1})\sinh(b\mu_{n3})\\&-\mu_{n3}\sinh(b\mu_{n1})\cosh(b\mu_{n3}))\\&+\alpha_n^2(\mu_{n1}\cosh(b\mu_{n1})\sinh(b\mu_{n3})(v\mu_{n1}^2-(v-2)\mu_{n3}^2)\\&+\mu_{n3}\sinh(b\mu_{n1})\cosh(b\mu_{n3})((v-2)\mu_{n1}^2-v\mu_{n3}^2))\\&+\mu_{n1}^2\mu_{n3}^2(\mu_{n3}\sinh(b\mu_{n1})\cosh(b\mu_{n3})\\&-\mu_{n1}\cosh(b\mu_{n1})\sinh(b\mu_{n3}))=0.\end{aligned} \quad (18)$$

Case of the SCSF plate:

$$\begin{aligned}&(2-v)v\alpha_n^4\left(\left(\mu_{n1}^2+\mu_{n3}^2\right)\sinh(b\mu_{n1})\sinh(b\mu_{n3})\right.\\&-2\mu_{n1}\mu_{n3}\cosh(b\mu_{n1})\cosh(b\mu_{n3})\\&\left.+2\mu_{n1}\mu_{n3}\right)+\alpha_n^2(2\mu_{n1}\mu_{n3}\left(\mu_{n1}^2+\mu_{n3}^2\right)\\&\times\cosh(b\mu_{n1})\cosh(b\mu_{n3})-2\mu_{n1}\mu_{n3}\\&\times\left(\mu_{n1}^2+\mu_{n3}^2\right)-\sinh(b\mu_{n1})\sinh(b\mu_{n3})\\&\times(-2(v-2)\mu_{n1}^2\mu_{n3}^2+v\mu_{n1}^4+v\mu_{n3}^4))\\&+\mu_{n1}\mu_{n3}(\mu_{n1}\mu_{n3}(\mu_{n1}^2+\mu_{n3}^2)\sinh(b\mu_{n1})\sinh(b\mu_{n3})\\&-2\mu_{n1}^2\mu_{n3}^2\cosh(b\mu_{n1})\cosh(b\mu_{n3})+\mu_{n1}^4+\mu_{n3}^4)=0.\end{aligned} \quad (19)$$

Case of the SFSF plate:

$$\begin{aligned}&\alpha_n^4(-v^2\sinh(b\mu_{n1})\sinh(b\mu_{n3})\mu_{n1}^6\\&-2(-2+v)v(-1+\cosh(b\mu_{n1})\cosh(b\mu_{n3}))\mu_{n1}^5\mu_{n3}\\&+(-2+v)(2+3v)\sinh(b\mu_{n1})\sinh(b\mu_{n3})\mu_{n1}^4\mu_{n3}^2\\&+8(-1+\cosh(b\mu_{n1})\cosh(b\mu_{n3}))\mu_{n1}^3\mu_{n3}^3\\&+(-2+v)(2+3v)\sinh(b\mu_{n1})\sinh(b\mu_{n3})\mu_{n1}^2\mu_{n3}^4\\&-2(-2+v)v(-1+\cosh(b\mu_{n1})\cosh(b\mu_{n3}))\mu_{n1}\mu_{n3}^5\\&-v^2\sinh(b\mu_{n1})\sinh(b\mu_{n3})\mu_{n3}^6)\\&+\mu_{n1}^4\mu_{n3}^4(-2\mu_{n1}\mu_{n3}+2\cosh(b\mu_{n1})\cosh(b\mu_{n3})\mu_{n1}\mu_{n3}\\&-\sinh(b\mu_{n1})\sinh(b\mu_{n3})\left(\mu_{n1}^2+\mu_{n3}^2\right))\\&-(-2+v)^2v^2\alpha_n^8(2\mu_{n1}\mu_{n3}\\&-2\cosh(b\mu_{n1})\cosh(b\mu_{n3})\mu_{n1}\mu_{n3}\\&+\sinh(b\mu_{n1})\sinh(b\mu_{n3})\left(\mu_{n1}^2+\mu_{n3}^2\right))\\&-2(-2+v)v\alpha_n^6(2\mu_{n1}\mu_{n3}\left(\mu_{n1}^2+\mu_{n3}^2\right)\\&-2\cosh(b\mu_{n1})\cosh(b\mu_{n3})\mu_{n1}\mu_{n3}\left(\mu_{n1}^2+\mu_{n3}^2\right)\end{aligned}$$

$$
\begin{aligned}
&+\sinh(b\mu_{n1})\sinh(b\mu_{n3})\\
&\times\left(\nu\mu_{n1}^4-2(-2+\nu)\mu_{n1}^2\mu_{n3}^2+\nu\mu_{n3}^4\right))\\
&+2\alpha_n^2\mu_{n1}^2\mu_{n3}^2(2\mu_{n1}\mu_{n3}\left(\mu_{n1}^2+\mu_{n3}^2\right)\\
&-2\cosh(b\mu_{n1})\cosh(b\mu_{n3})\mu_{n1}\mu_{n3}\left(\mu_{n1}^2+\mu_{n3}^2\right)\\
&+\sinh(b\mu_{n1})\sinh(b\mu_{n3})\\
&\times\left(\nu\mu_{n1}^4-2(-2+\nu)\mu_{n1}^2\mu_{n3}^2+\nu\mu_{n3}^4\right)))=0. \qquad (20)
\end{aligned}
$$

Only the non-dimensional frequency parameter in the case of the SSSS plate can be determined explicitly as

$$
\Omega=\sqrt{\frac{\hat{k}_1+\pi^2\left(m^2+n^2\beta^2\right)\left(\pi^2\left(m^2+n^2\beta^2\right)+\hat{k}_2\right)}{1+\pi^2\left(m^2+n^2\beta^2\right)\psi}}, \qquad (21)
$$

where m and n are the number of half-waves on the x axis and y axis, $\beta=a/b$, $\psi=I/a^2\rho h$, $\hat{k}_1=a^4k_1/D$, $\hat{k}_2=a^2k_2/D$, and $\Omega=\omega a^2\sqrt{\rho h/D}$.

Table 1. Boundary conditions.

Types of boundary conditions	$y=0$ or $y=b$
Simply supported edge (S)	$W=0, \frac{\partial^2 W}{\partial y^2}=0$
Clamped edge (C)	$W=0, \frac{\partial W}{\partial y}=0$
Free edge (F)	$\frac{\partial^2 W}{\partial y^2}+\nu\frac{\partial^2 W}{\partial x^2}=0,$ $\frac{\partial^3 W}{\partial y^3}+(2-\nu)\frac{\partial^3 W}{\partial x^2\partial y}=0$

The roots of other cases can be found through computer programming using Newton's method. Table 2 presents the first six non-dimensional frequency parameters of the SSSC, SCSC, SSSF, SCSF and SFSF plates with different aspect ratios. To ensure the correctness of the roots we obtained, we include a comparison with those from Ref. [31]. The present solutions show excellent agreement with the corresponding results.

Table 2. Non-dimensional frequency parameter $\Omega=\omega a^2\sqrt{\rho h/D}$ with different aspect ratios when $\nu=0.3$.

	a/b		Ω_1	Ω_2	Ω_3	Ω_4	Ω_5	Ω_6
	2/3	Present	15.578278	31.072360	44.564354	55.392604	59.462652	83.605970
S		Ref. [31]	15.5783	31.0724	44.5644	55.3926	59.4627	83.6060
S	1.0	Present	23.646320	51.674275	58.646363	86.134464	100.269797	113.228097
S		Ref. [31]	23.6463	51.6743	58.6464	86.1345	100.2698	113.2281
C	1.5	Present	42.527803	69.003124	116.267118	120.995553	147.635318	184.100612
		Ref. [31]	42.5278	69.0031	116.2671	120.9956	147.6353	184.1006
	2/3	Present	17.372998	35.344498	45.429418	62.054376	62.313113	88.804681
S		Ref. [31]	17.3730	35.3445	45.4294	62.0544	62.3131	88.8047
C	1.0	Present	28.950850	54.743071	69.327014	94.585278	102.216191	129.095537
S		Ref. [32]	28.9509	54.7431	69.3270	94.5853	102.2162	129.0955
C	1.5	Present	56.348065	78.983583	123.171909	146.267697	170.111212	189.121942
		Ref. [31]	56.3481	78.9836	123.1719	146.2677	170.1112	189.1219
	2/3	Present	10.671167	18.299546	33.697353	40.130704	48.408211	57.592936
S		Ref. [31]	10.6712	18.2995	33.6974	40.1307	48.4082	57.5929
S	1.0	Present	11.684537	27.756345	41.196651	59.065511	61.860613	90.294085
S		Ref. [31]	11.6845	27.7563	41.1967	59.0655	61.8606	90.2941
F	1.5	Present	13.711087	43.572256	47.857146	81.478911	92.692466	124.563530
		Ref. [31]	13.7111	43.5723	47.8571	81.4789	92.6925	124.5635
	2/3	Present	10.975240	20.335536	37.955208	40.271721	49.731728	64.188935
S		Ref. [31]	10.9752	20.3355	37.9552	40.2717	49.7317	64.1889
C	1.0	Present	12.687360	33.065090	41.701929	63.014831	72.397563	90.611372
S		Ref. [31]	12.6874	33.0651	41.7019	63.0148	72.3976	90.6114
F	1.5	Present	16.822470	45.302426	61.017760	92.307320	93.829341	141.783370
		Ref. [31]	16.8225	45.3024	61.0178	92.3073	93.8293	141.7834
	2/3	Present	9.698322	12.981340	22.953493	39.105198	40.356046	42.684699
S		Ref. [31]	9.6983	12.9813	22.9535	39.1052	40.3560	42.6847
F	1.0	Present	9.631385	16.134777	36.725642	38.944959	46.738147	70.740108
S		Ref. [31]	9.6314	16.1348	36.7256	38.9450	46.7381	70.7401
F	1.5	Present	9.558176	21.619198	38.721406	54.844349	65.792214	87.626157
		Ref. [31]	9.5582	21.6192	38.7214	54.8443	65.7922	87.6262

3. Frequency spectra for Lévy plates

Here, we have improved the frequency spectra of the Lévy plates by introducing the aspect ratio and non-dimensional frequency parameter. The x axis of the spectra represents the aspect ratio, while the y axis represents the non-dimensional frequency parameter. This enhancement makes the frequency spectra more universally applicable. In frequency spectra, Ω can be divided into four symmetry classes according to the geometric symmetry of the rectangular plate. In Eq. (21), when both m and n are odd, this represents the symmetric-symmetric (SS) symmetry class. When m is odd and n is even, it represents the symmetric-antisymmetric (SA) symmetry class. When m is even and n is odd, it represents the

antisymmetric-symmetric (AS) symmetry class. When both m and n are even, it represents the antisymmetric-antisymmetric (AA) symmetry class. In order to analyze the influence that is imposed on the frequency spectra by changing the foundation parameters and rotary inertia, we calculated the spectra of Lévy plates under six different boundary conditions for a total of 108 combinations, with rotary inertia parameter ψ taking values of 0 or 10^{-2}, and foundation parameters $\hat{k}_1$ and $\hat{k}_2$ taking values of 0, 10^2, 10^3. For the SSSS plate, we obtained the frequency spectra in the interval $(1,2)$ from Eq. (21). For other boundary conditions of plates, we calculated the first 70 mode frequencies at each aspect ratio, with the aspect ratio values taken as 1.0, 1.1, 1.2, 1.3, 1.4, 1.5, 1.6, 1.7, 1.8, and 1.9.

3.1. Frequency spectra without rotary inertia

Figure 2 depicts the frequency spectra of the SSSS plate on a two-parameter elastic foundation without rotary inertia. It shows that regardless of how the foundation parameters change, the frequency levels of the same symmetry class and different symmetry classes also cross each other, with avoided crossing absence in the spectra of SSSS plates. As predicted by the BT conjecture, level clustering has occurred. Comparing Figs. 2(a) and 2(c) and comparing Figs. 2(b) and 2(d), we can observe that when $\hat{k}_1$ increases from 0 to 10^3, the spectra hardly change, only experiencing slight translation. It is due to foundation parameter $\hat{k}_1 = a^4 k_1/D$, where k_1 represents the Winkler parameter, which signifies the foundation's resistance to transverse translations and produces a minimal impact on the frequency. Comparing Figs. 2(a) and 2(b) and comparing Figs. 2(c) and 2(d) reveals that the parameter $\hat{k}_2$ causes an apparent change in the shape of the frequency spectra, where $\hat{k}_2 = a^2 k_2/D$ and k_2 is the shear parameter, representative of the foundation's resistance to rotational deformations. This precisely illustrates the advantage of the two-parameter model, as k_2 has a more significant impact on frequency compared to parameter k_1.[32] The same phenomenon observed under the SSSS case has been observed in the frequency spectra of plates under other boundary conditions. This verifies the universality of the BT conjecture in Lévy plates. Table 3 presents the mean square error (MSE) between spectra for different values of $\hat{k}_1$ and $\hat{k}_2$. It is evident that $\hat{k}_2$ has a greater impact on the spectra compared to $\hat{k}_1$, validating our observations above.

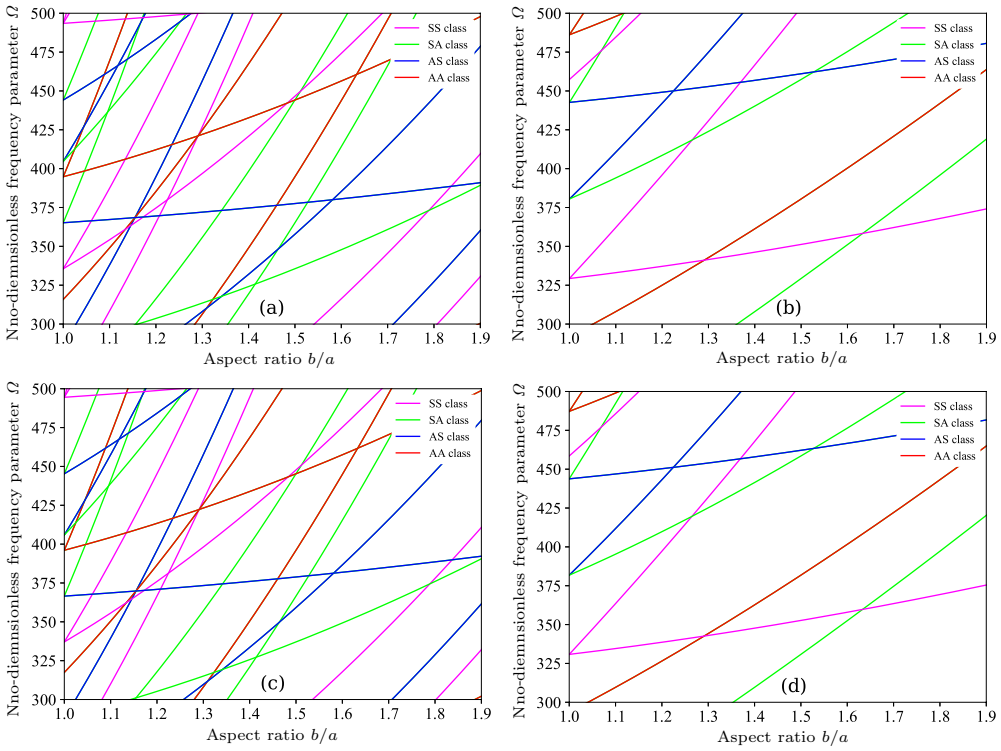


Fig. 2. Frequency spectra of the SSSS plate on a two-parameter elastic foundation without rotary inertia ($\psi = 0$). (a) $\hat{k}_1 = 0$, $\hat{k}_2 = 0$; (b) $\hat{k}_1 = 0$, $\hat{k}_2 = 10^3$; (c) $\hat{k}_1 = 10^3$, $\hat{k}_2 = 0$; (d) $\hat{k}_1 = 10^3$, $\hat{k}_2 = 10^3$.

Table 3. The MSE of the frequency spectra for different values of $\hat{k}_1$ and $\hat{k}_2$.

$\hat{k}_1$ \ $\hat{k}_2$	0	10	10^2	10^3	10^4
0	0.0000	23.7869	1776.8889	66242.1306	1164483.9884
10	0.0051	24.2668	1779.5803	66248.7025	1164492.8215
10^2	0.4904	28.8990	1803.8854	66307.8556	1164572.3916
10^3	37.3051	100.0187	2054.6538	66899.9600	1165367.3213
10^4	1713.1125	1961.3752	5096.3006	72874.7907	1173319.4342

3.2. The impact of rotary inertia on the frequency spectra

Figure 3 shows the frequency spectra of the SSSS plate on a two-parameter elastic foundation with $\psi = 10^{-2}$, $\hat{k}_1 = 0$, $\hat{k}_2 = 0$, which show that the BT conjecture still holds. Rotary inertia parameters ψ depend on the thickness of the plate. In Lévy plates, ψ have been set to a very small value of 10^{-2}, which has a noticeable impact on the spectra. Compared to Fig. 2(a), Fig. 3(a) reveals that rotary inertia causes the distance between two consecutive frequency levels to decrease and the frequency levels to become concentrated. The non-dimensional frequency parameter of Fig. 3(a) ranges from 100 to 260. When focusing on the interval $[150, 200]$, as shown in Fig. 3(b), it is the same as Fig. 2(a). This situation occurs not only in the SSSS plate but also in the other five boundary conditions. According to Eq. (5), the rotary inertia parameter scales the frequency parameter in the SSSS plate. The explicit expressions for frequencies under other boundary conditions cannot be obtained. This phenomenon in the spectra tells us that how the rotary inertia parameter affects the frequencies is the same for different boundary conditions, namely, scaling the frequency parameters. So, whether the rotary inertia exists or not, level clustering also exists, as predicted by the BT conjecture.

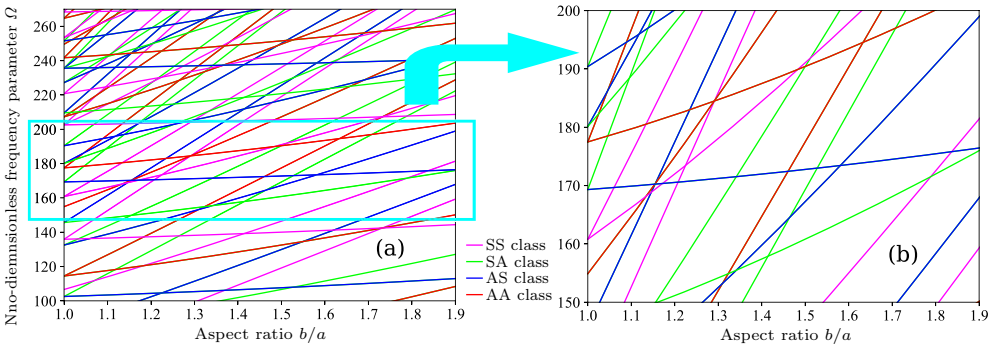


Fig. 3. The frequency spectra of the SSSS plate on a two-parameter elastic foundation with $\psi = 10^{-2}$.

4. Distribution of the nearest neighbor level spacing ratios

In the BT conjecture, the nearest neighbor frequency level spacing statistic $s_n = f_{n+1} - f_n$ is used to describe the distribution of the distance between two consecutive frequency levels, where f_n can be understood as the normal-mode frequency. Afterward, s_n has been widely used in the quantum field.[33–37] Oganesyan and Huse proposed a new statistic $\widetilde{r}_n$ to address the computational challenges posed by the large calculation volume in many-body problems.[38] The nearest neighbor level spacing ratios statistic $\widetilde{r}_n$ defined by

$$0 \le \widetilde{r}_n = \frac{\min(s_n, s_{n-1})}{\max(s_n, s_{n-1})} = \min\left(r_n, \frac{1}{r_n}\right) \le 1,$$

where

$$r_n = \frac{s_n}{s_{n-1}}.$$

This $\widetilde{r}_n$ statistic has the advantage of its low computational cost, allows a more transparent comparison with experiments, and is more precise than the s_n statistic. We redefine the $\widetilde{r}_n$ statistic in Lévy plates as

$$\widetilde{r}_n = \frac{\Omega_{n+1} - \Omega_n}{\Omega_n - \Omega_{n-1}},$$

where $\{\Omega_n\}$ is the set of ordered non-dimensional frequency parameters of the Lévy plates. We calculate $P(\widetilde{r})$ (the distribution of the $\widetilde{r}_n$ statistic) for Lévy plates under six different boundary conditions, resulting in a total of 108 combinations through the roots obtained from Eqs. (15)–(20). The rotary inertia parameter ψ takes values of 0 or 10^{-2}, while the foundation parameters $\hat{k}_1$ and $\hat{k}_2$ take values of 0, 10^2, and 10^3. At least the first five thousand non-dimensional frequency parameters were calculated for each case.

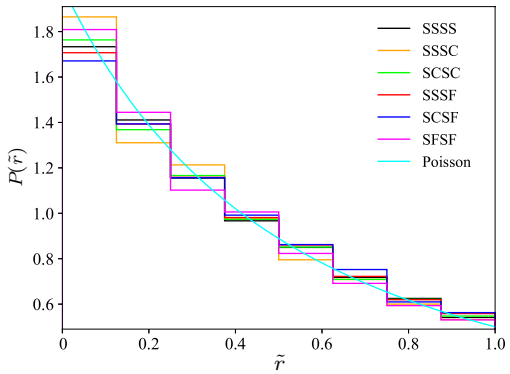


Fig. 4. Distribution of the $\widetilde{r}_n$ statistic (profile histograms) for Lévy plates under six different boundary conditions, compared with Poisson distributions.

Figure 4 shows $P(\widetilde{r})$ under six different boundary conditions, compared with the distribution of the ratios of consecutive level spacing for Poisson statistics, which is $P_p(\widetilde{r}) = 2/(1+r^2)$.[39,40] For the SSSS plate, $\psi = 0$, $\hat{k}_1 = 0$, $\hat{k}_2 = 0$. For the SCSC plate, $\psi = 0$, $\hat{k}_1 = 10^3$, $\hat{k}_2 = 0$. For the SSSC plate, $\psi = 0$, $\hat{k}_1 = 10^3$, $\hat{k}_2 = 10^3$. For the SSSF plate, $\psi = 10^{-2}$, $\hat{k}_1 = 0$, $\hat{k}_2 = 0$. For the SCSF plate, $\psi = 10^{-2}$,

$\hat{k}_1 = 0$, $\hat{k}_2 = 10^3$. For the SFSF plate, $\psi = 10^{-2}$, $\hat{k}_1 = 10^3$, $\hat{k}_2 = 10^3$. The $\widetilde{r}_n$ statistic overlaps with the Poisson distribution in six different situations. After extensive numerical calculations, regardless of variations in boundary conditions, rotary inertia, or foundation parameters, the $\widetilde{r}_n$ statistic always follows a Poisson distribution. The Poisson distribution is universal in Lévy plates.

Figure 5 shows the influence of the values of N on $P(\widetilde{r})$, in which N represents the maximum number of terms considered for non-dimensional frequency parameters for each aspect ratio. When N is set to 200, the shape of $P(\widetilde{r})$ starts to resemble a Poisson distribution, and when N is set to 400, it closely resembles a Poisson distribution.

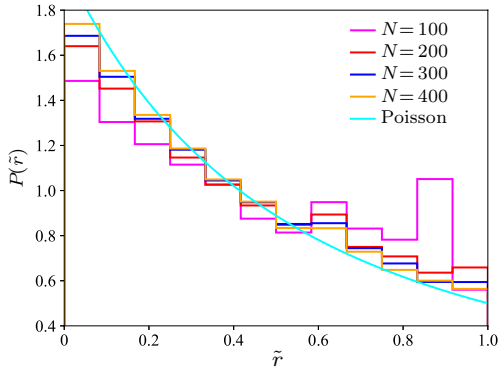


Fig. 5. Distribution of the $\widetilde{r}_n$ statistic of the SSSS plate at different values of N, in which $\psi = 10^{-2}$, $\hat{k}_1 = 10^3$, $\hat{k}_2 = 10^3$, compared with Poisson distributions.

5. Summary and discussion

Frequency spectra of the Lévy plates on a two-parameter foundation have been obtained using the Hamiltonian approach. As predicted by the BT conjecture, level clustering occurs in the spectra. The impact of boundary conditions, rotary inertia, and foundation parameters on the frequency spectra has been considered. The parameter k_1 only results in a slight shift in the spectra. Parameter k_2 leads to a fundamental change in the shape of the spectra. Rotary inertia compacts the frequency and scales the frequency spectra in Lévy plates. The level clustering corresponds to Poisson behavior of $P(\widetilde{r})$. The distribution of nearest neighbor frequency level spacing ratios $P(\widetilde{r})$ for Lévy plates was calculated in 108 different cases, and without exception, all of them followed a Poisson distribution, and the Poisson distribution shape can be demonstrated with a minimal sample size. The universality of the Poisson distribution holds in Lévy plates, and then the BT conjecture has been extended to Lévy plates.

In the BT conjecture, the prerequisite for manifesting a Poisson distribution is that there is no correlation between the energy levels. In Eq. (13), the free vibration of the Lévy plates is decoupled into a variety of single-degree-of-freedom systems in modal space. Equation (14) consists of mode functions containing modal frequencies. Due to the orthogonality of the sine function systems, there is no energy exchange between different modes; in other words, the frequencies are mutually independent of each other. So, the Poisson distribution appears in the frequency of the Lévy plates. The presence of avoided crossing in the FFFF plate may be due to the correlation between frequencies. The difference between free and simply supported boundary conditions is that when a bending ray reaches a free boundary, in addition to the reflected ray, a new ray that follows the boundary path exclusively emerges.[41] The new ray accounts for the correlation between frequencies in the FFFF plate. This phenomenon inspires the solving of vibration problems of plates with complex boundary conditions using the symplectic superposition method.

Acknowledgements

Project supported by the National Natural Science Foundation of China (Grant Nos. 12261064 and 11861048), the Natural Science Foundation of Inner Mongolia, China (Grant No. 2021MS01004), and the Innovation Program for Graduate Education of Inner Mongolia University (Grant No. 11200-5223737).

References

[1] Brody T A, Flores J, French J B, Mello P A, Pandey A and Wong S S M 1981 *Rev. Mod. Phys.* **53** 385
[2] Müller S, Heusler S, Altland A, Braun P and Haake F 2009 *New J. Phys.* **11** 103025
[3] Porter C E 1965 *Fluctuations of Quantal Spectra* (New York: Academic Press) p. 8
[4] Berry M V, Tabor and Ziman J M 1977 *Proc. R. Soc.* **356** 375
[5] Casati G, Chirikov B V and Guarneri I 1985 *Phys. Rev. Lett.* **54** 1350
[6] Bohigas O, Giannoni M J and Schmit C 1984 *Phys. Rev. Lett.* **52** 1
[7] Mehta M L 1990 *Random Matrix Theory*, 3rd Edn. (New York: Springer) p. 13
[8] Stöckmann H J and Stein J 1990 *Phys. Rev. Lett.* **64** 2215
[9] Frank O and Eckhardt B 1996 *Phys. Rev. E* **53** 4166
[10] Mohammadesmaeili R, Motaghian S and Mofid M 2021 *Eur. J. Mech. A Solids* **88** 104274
[11] Nguyen P, Pham Q H, Tran T T and Nguyen T 2022 *Ain Shams Eng. J.* **13** 101615
[12] Warburton G B and Edney S L 1984 *J. Sound Vib.* **95** 537
[13] Leissa A 1969 *Vibration of Plates* (NASA: Scientific and Technical Information Division)
[14] Biancolini M E, Brutti C and Reccia l 2005 *J. Sound Vib.* **288** 321
[15] Ellegaard C, Guhr T, Lindemann K, Lorensen H Q, Nygård J and Oxborrow M 1995 *Phys. Rev. Lett.* **75** 1546
[16] Bertelsen P, Ellegaard C and Hugues E 2000 *Eur. Phys. J. B* **15** 18
[17] Andersen A, Ellegaard C, Jackson A D and Schaadt K 2001 *Phys. Rev. E* **63** 066204
[18] Sondergaard, Niels and Tanner Gregor 2002 *Phys. Rev. E* **66** 066211
[19] Gregor Tanner and Niels Søndergaard 2007 *J. Phys. A: Math. Theor.* **40** R443
[20] López-González J L, Franco-Villafañe J A, Méndez-Sánchez R A, Zavala-Vivar G, Flores-Olmedo E, Arreola-Lucas A and Báez G 2021 *Phys. Rev. E* **103** 043004
[21] Timoshenko SP and Woinowsky-Krieger SW 1959 *Theory of plates and shells* (New York: McGraw-Hill) p. 180
[22] Reddy J N 2007 *Theory and Analysis of Elastic plates and Shells*, 2nd Edn. (New York: CRC Press) p. 331
[23] Hetenyi Miklos 1946 *Beams on Elastic Foundation: Theory with Applications in the Fields of Civil and Mechanical Engineering* (Ann Arbor: University of Michigan Press) p. 179

[24] Qiao Y F, Hou G L and Chen A 2021 *Appl. Math. Model.* **89** 1124
[25] Qiao Y F, Hou G L and Chen A 2021 *Appl. Math. Comput.* **400** 126043
[26] Sun Z Q, Hou G L, Qiao Y F and Liu J C 2023 *Chin. Phys. B* **33** 016107
[27] Yao W A, Zhong W X and Lim C W 2009 *Symplectic Elasticity* (Singapore: World Scientific) p. 71
[28] Zhong Y, Li R, Liu Y M and Tian B 2009 *Int. J. Solids Struct.* **46** 2506
[29] Su X, Bai E and Chen A 2021 *Int. J. Struct. Stab. Dyn.* **21** 2150122
[30] Su X and Bai E 2022 *J. Vib. Control.* **28** 3
[31] Leissa A W 1973 *J. Sound Vib.* **31** 257
[32] Omurtag M H and Kadıōlu F 1998 *Comput. Struct.* **67** 253
[33] Matsushita T and Terasaka T 1984 *Chem. Phys. Lett.* **105** 511
[34] Richens P J and Berry M V 1981 *Physica D* **2** 495
[35] Robnik M 1987 *J. Phys. A: Math. Gen.* **20** L495
[36] Dietz B and Haake F 1990 *Z. Phys. B* **80** 153
[37] Pechukas P 1983 *Phys. Rev. Lett.* **51** 943
[38] Oganesyan V and David A H 2007 *Phys. Rev. B* **75** 155111
[39] Atas Y Y, Bogomolny E, Giraud O and Roux G 2013 *Phys. Rev. Lett.* **110** 084101
[40] Atas Y Y, Bogomolny E, Giraud O and Roux G 2013 *J. Phys. A: Math. Theor.* **46** 355204
[41] Bogomolny E and Hugues E 1998 *Phys. Rev. E* **57** 5404